Hindawi
Mathematical Problems in Engineering
Volume 2019, Article ID 3163702, 10 pages
https://doi.org/10.1155/2019/3163702

Research Article

Numerical Approximation of the Space Fractional Cahn-Hilliard Equation

Zhifeng Weng, Langyang Huang, and Rong Wu

Fujian Province University Key Laboratory of Computation Science, School of Mathematical Sciences, Huaqiao University, Quanzhou 362021, China

Correspondence should be addressed to Zhifeng Weng; zfwmath@163.com

Received 9 January 2019; Revised 9 March 2019; Accepted 17 March 2019; Published 1 April 2019

Academic Editor: Francisco R. Villatoro

In this paper, a second-order accurate (in time) energy stable Fourier spectral scheme for the fractional-in-space Cahn-Hilliard (CH) equation is considered. The time is discretized by the implicit backward differentiation formula (BDF), along with a linear stabilized term which represents a second-order Douglas-Dupont-type regularization. The semidiscrete schemes are shown to be energy stable and to be mass conservative. Then we further use Fourier-spectral methods to discretize the space. Some numerical examples are included to testify the effectiveness of our proposed method. In addition, it shows that the fractional order controls the thickness and the lifetime of the interface, which is typically diffusive in integer order case.

1. Introduction

The Cahn-Hilliard model [1, 2] was originated from a phase-separation model in a binary alloy. The Cahn-Hilliard model has been widely used in many complicated moving interface problems in materials science and fluid dynamics through a phase-field approach [3–5]. Hence, it is important to study the physical properties of Cahn-Hilliard equations by accurate and efficient numerical algorithms. The numerical analysis of Cahn-Hilliard equations and the references therein have been studied in the past [3, 6, 7].

However, in the original formulation of the physical model [1], nonlocal interactions were parts of CH model, but in the subsequent mathematical literatures CH model was approximated by local one by assuming slow spatial variations. In recent years, fractional phase-field models have attracted the attention of many researchers, and a relevant number of works [8–12] have been devoted to the mathematical/numerical analysis of the space (time) fractional phase-field models. The space fractional phase-field models can provide a more accurate description of the formation and phase change mechanism by considering the long-range interactions among particles. So it is necessary to obtain high accuracy numerical solutions and design numerical methods for the space fractional phase-field models that satisfy the energy decays with respect to time.

In this paper, we focus on the following fractional-in-space Cahn-Hilliard (CH) equation [9]:

$$\frac{\partial u}{\partial t} = \Delta\left(\epsilon^2 (-\Delta)^{\alpha/2} u + f(u)\right), \quad (\mathbf{x}, t) \in \Omega \times (0, T], \tag{1}$$
$$u(\mathbf{x}, 0) = u_0(\mathbf{x}), \quad \mathbf{x} \in \Omega,$$

where Ω is a bounded regular domain in R^d ($d = 1, 2, 3$), and $T > 0$ denotes a finite time. For the above equation, we impose the periodic or following homogeneous Neumann boundary conditions

$$\mathbf{n} \cdot \nabla u = 0, \qquad \mathbf{n} \cdot \nabla\left(f(u) + \epsilon^2 (-\Delta)^{\alpha/2} u\right) = 0, \tag{2}$$

on Ω. Here $\mathbf{n}$ is the unit outward normal vector of the domain Ω. The function u denotes the concentration for one of the two metallic components of the alloy, and ϵ is the interfacial energy in a phase-separation phenomenon. The nonlinear

function $f(u) = F'(u)$ and $F(u) = (1/4)(u^2 - 1)^2$ is a given energy potential, taking its global minimum value at $u = -1$ and $u = 1$. In other words, the values -1 and 1 of the function u prevail in Ω whereas the transition between them forms a thin interface layer.

The fractional CH equation (1) can be viewed as an H^{-1}-gradient flow of the following fractional analogue version of Ginzburg-Landau free energy functional [10]:

$$E^{\alpha}(u) = \int_{\Omega} \left(\frac{\epsilon^2}{2} \left| (-\Delta)^{\alpha/4} u \right|^2 + F(u) \right) d\mathbf{x}. \tag{3}$$

The same as the standard CH equation [1], one intrinsic property of the fractional-in-space CH equation is energy-decay property in sense of

$$\frac{d}{dt} E^{\alpha}(u) = -\int_{\Omega} \left| \nabla \left(\epsilon (-\Delta)^{\alpha/2} u + f(u) \right) \right|^2 d\mathbf{x} \leq 0. \tag{4}$$

Another intrinsic property of the fractional-in-space CH equation, as well as the standard CH equation, is the law of conservation of mass

$$\frac{d}{dt} M(u) = \frac{d}{dt} \int_{\Omega} u(\mathbf{x}, t)\, d\mathbf{x} = 0. \tag{5}$$

Comparing with the well-known classic CH equation [1], the fractional-in-space CH equation is equipped with a nonlocal diffusion operator and can describe more practical phenomena for modeling phase transitions of microstructures in materials. On the other hand, it evidently brings more computational costs in numerical simulations; thus efficient and accurate numerical methods are highly desired. Recently, Bosch and Stoll [8] used Fourier spectral method for fractional vector-valued CH model combined with an implicit first-order convex splitting scheme. Numerical tests showed the superiority of the proposed fractional CH inpainting approach over its nonfractional version. Ainsworth and Mao [9] proposed a first-order semi-implicit Fourier-Galerkin scheme for solving the 2D model (1) and detailed theoretical research and simulation studies were given. Weng [11] et al. proposed an unconditionally energy stable nonlinear Fourier spectral scheme for model (1) by introducing a stabilizing term.

In our previous work [11], we have proposed second-order unconditionally energy stable Fourier spectral scheme for fractional-in-space Cahn-Hilliard equation using the Crank-Nicolson methodology and nonlinear stabilized term. In this paper, new schemes are proposed combining the implicit backward differentiation formula and stabilized term. Mainly, the new schemes are three-level schemes, and the stabilized term is linear. The newly proposed BDF schemes are unconditionally energy stable second-order accurate in time. Then we develop a Fourier spectral scheme to effectively treat the significantly increased memory requirement and computational complexity for space fractional CH models. The energy stability and mass conservation will be proven in the semidiscretized case in time. Compared with the literature [11], our method is more efficient for solving fractional-in-space Cahn-Hilliard in numerical experiments.

The rest of the paper is organized as follows. In Section 2, we develop the numerical schemes and prove their unconditional energy stability and mass conservation in the semidiscretized case in time. In Section 3, we present some numerical simulations to demonstrate the accuracy and efficiency of the proposed method. Finally, some concluding remarks are presented in Section 4.

2. Numerical Schemes

In this section, an unconditionally energy stable and mass conservation of the second order BDF-type scheme in time will be proven. Then we will propose fully discrete scheme based on the implicit backward difference scheme for the time and Fourier spectral method for the space to solve the fractional equation (1).

2.1. An Unconditionally Energy Stable and Mass Conservation Semidiscrete Scheme. First, we use a finite difference method to discretize the time direction of the fractional CH equation (1). Let $t_m = m\tau$, $m = 0, 1, \ldots, M$, where $\tau = T/M$. The new second-order scheme can be written as

$$\begin{aligned} &\frac{3u^{m+1} - 4u^m + u^{m-1}}{2\tau} \\ &\quad = \Delta \left(\epsilon^2 (-\Delta)^{\alpha/2} u^{m+1} + \left(u^{m+1} \right)^3 - 2u^m + u^{m-1} \right) \\ &\qquad - A\tau\Delta^2 \left(u^{m+1} - u^m \right), \end{aligned} \tag{6}$$

where $A\tau\Delta^2(u^{m+1} - u^m)$ is a stabilizing term with $A > 0$, and u^1 is approximated by the following unconditionally stable Crank-Nicolson scheme [11]:

$$\begin{aligned} \frac{u^1 - u^0}{\tau} &= \Delta \left(\epsilon^2 (-\Delta)^{\alpha/2} u^{1/2} + f^{1/2} \right) \\ &\quad - \frac{1}{2} \Delta \left[\left(u^1 - u^0 \right)^2 u^{1/2} \right], \end{aligned} \tag{7}$$

where $u^{1/2} = (u^0 + u^1)/2$ and $f^{1/2} = (f^0 + f^1)/2$.

For this semidiscretized problem, we have the following energy stability estimate, which is a slight modification of the Theorem 4.1 for the standard CH equation in [13].

Theorem 1. *For $m \geq 1$, define*

$$\begin{aligned} \mathbb{E}^{\alpha} \left(u^{m+1}, u^m \right) &= E^{\alpha} \left(u^{m+1} \right) + \frac{1}{4\tau} \left\| u^{m+1} - u^m \right\|_{-1}^2 \\ &\quad + \frac{1}{2} \left\| u^{m+1} - u^m \right\|_0^2, \end{aligned} \tag{8}$$

where $E^{\alpha}(u) = (\epsilon^2/2)\|(-\Delta)^{\alpha/4} u\|^2 + (1/4)\|u\|_{L^4}^4 - (1/2)\|u\|^2$ and suppose $A \geq 1/16$. Then the semidiscrete scheme (6) is unconditionally energy stable, i.e., for all $\tau > 0$

$$\mathbb{E}^{\alpha} \left(u^{m+1}, u^m \right) \leq \mathbb{E}^{\alpha} \left(u^m, u^{m-1} \right). \tag{9}$$

Here $\|u^m\|_{-1}^2 := (u^m, (-\Delta)^{-1} u_m)$ is inner product of $H^{-1}(\Omega)$.

Proof. We use $\|\cdot\|_2$ to denote the L^2 norm and $(\cdot,\cdot)$ to the inner product in L^2. Taking the L^2 inner product for (6) with $(-\Delta)^{-1}(u^{m+1}-u^m)$ yields

$$\begin{aligned}
&\left(\frac{3u^{m+1}-4u^m+u^{m-1}}{2\tau},(-\Delta)^{-1}\left(u^{m+1}-u^m\right)\right)\\
&+\epsilon^2\left((-\Delta)^{1+\alpha/2}u^{m+1},(-\Delta)^{-1}\left(u^{m+1}-u^m\right)\right)\\
&+\left((-\Delta)\left(u^{m+1}\right)^3,(-\Delta)^{-1}\left(u^{m+1}-u^m\right)\right)\\
&+\left(\Delta\left(2u^m-u^{m-1}\right),(-\Delta)^{-1}\left(u^{m+1}-u^m\right)\right)\\
&+A\tau\left((-\Delta)^2\left(u^{m+1}-u^m\right),(-\Delta)^{-1}\left(u^{m+1}-u^m\right)\right)\\
&=J_1+J_2+J_3+J_4+J_5=0.
\end{aligned}\tag{10}$$

Now we estimate the terms J_1-J_5, respectively. For the time difference term, by the definition of the norm $\|u^m\|_{-1}^2$, it is easy to obtain

$$\begin{aligned}
J_1&=\frac{1}{2\tau}\left(3u^{m+1}-4u^m+u^{m-1},(-\Delta)^{-1}\left(u^{m+1}-u^m\right)\right)\\
&=\frac{1}{4\tau}\left(6u^{m+1}-8u^m+2u^{m-1},(-\Delta)^{-1}\left(u^{m+1}-u^m\right)\right)\\
&=\tau\left(\frac{5}{4}\left\|\frac{u^{m+1}-u^m}{\tau}\right\|_{-1}^2-\frac{1}{4}\left\|\frac{u^m-u^{m-1}}{\tau}\right\|_{-1}^2\right)\\
&\quad+\frac{\tau^3}{4}\left\|\frac{u^{m+1}-2u^m+u^{m-1}}{\tau^2}\right\|_{-1}^2.
\end{aligned}\tag{11}$$

For the highest-order diffusion, using the identity

$$(b,b-a)=\frac{1}{2}|b|^2-\frac{1}{2}|a|^2+\frac{1}{2}|b-a|^2,\tag{12}$$

we can obtain

$$\begin{aligned}
J_2&=\epsilon^2\left((-\Delta)^{1+\alpha/2}u^{m+1},(-\Delta)^{-1}\left(u^{m+1}-u^m\right)\right)\\
&=\frac{\epsilon^2}{2}\left(\left\|(-\Delta)^{\alpha/4}u^{m+1}\right\|^2-\left\|(-\Delta)^{\alpha/4}u^m\right\|^2\right)\\
&\quad+\frac{\epsilon^2}{2}\left\|(-\Delta)^{\alpha/4}\left(u^{m+1}-u^m\right)\right\|^2.
\end{aligned}\tag{13}$$

By virtue of the identity

$$\begin{aligned}
\left(b^3,b-a\right)&=\frac{1}{4}\left(|b|^4-|a|^4\right)+\frac{1}{4}\left|b^2-a^2\right|^2\\
&\quad+\frac{1}{2}|b(b-a)|^2,
\end{aligned}\tag{14}$$

the nonlinear term becomes

$$\begin{aligned}
J_3&=\left(\left(u^{m+1}\right)^3,\left(u^{m+1}-u^m\right)\right)\\
&=\frac{1}{4}\left(\left\|u^{m+1}\right\|_{L^4}^4-\left\|u^m\right\|_{L^4}^4\right)+\frac{1}{4}\left\|\left(u^{m+1}\right)^2-\left(u^m\right)^2\right\|^2\\
&\quad+\frac{1}{2}\left\|u^{m+1}\left(u^{m+1}-u^m\right)\right\|^2.
\end{aligned}\tag{15}$$

By means of the identity

$$(b,b-a)=\frac{1}{2}|b|^2-\frac{1}{2}|a|^2+\frac{1}{2}|b-a|^2,\tag{16}$$

the concave diffusive term turns out to be

$$\begin{aligned}
J_4&=-\left(2u^m-u^{m-1},u^{m+1}-u^m\right)\\
&=-\left(u^m,u^{m+1}-u^m\right)-\left(u^m-u^{m-1},u^{m+1}-u^m\right)\\
&=-\frac{1}{2}\left(\left\|u^{m+1}\right\|^2-\left\|u^m\right\|^2\right)+\frac{1}{2}\left\|u^{m+1}-u^m\right\|^2\\
&\quad+\left(u^{m+1}-2u^m+u^{m-1},u^{m+1}-u^m\right)\\
&\quad-\left\|u^{m+1}-u^m\right\|^2\\
&=-\frac{1}{2}\left\|u^{m+1}\right\|^2+\frac{1}{2}\left\|u^{m+1}-u^m\right\|^2\\
&\quad-\left(-\frac{1}{2}\left\|u^m\right\|^2+\frac{1}{2}\left\|u^m-u^{m-1}\right\|^2\right)\\
&\quad+\frac{1}{2}\left\|u^{m+1}-2u^m+u^{m-1}\right\|^2-\frac{1}{2}\left\|u^{m+1}-u^m\right\|^2.
\end{aligned}\tag{17}$$

Finally, the stabilizing term becomes

$$J_5=A\tau\left\|\nabla\left(u^{m+1}-u^m\right)\right\|^2.\tag{18}$$

For any $\sigma>0$ and the formula from the last row in J_4, in virtue of the Cauchy-Schwarz inequality, we have

$$\begin{aligned}
\frac{1}{2}\left\|u^{m+1}-u^m\right\|^2&\le\frac{1}{2}\left\|\nabla u^{m+1}-\nabla u^m\right\|\left\|u^{m+1}-u^m\right\|\\
&\le\frac{\tau}{4\sigma}\left\|\nabla u^{m+1}-\nabla u^m\right\|^2\\
&\quad+\frac{\sigma\tau}{4}\left\|\frac{u^{m+1}-u^m}{\tau}\right\|_{-1}^2
\end{aligned}\tag{19}$$

Putting everything together, we can get

$$\begin{aligned}
&\mathbb{E}^\alpha\left(u^{m+1},u^m\right)+\tau\left(1-\frac{\sigma}{4}\right)\left\|\frac{u^{m+1}-u^m}{\tau}\right\|_{-1}^2\\
&\quad+\tau\left(A-\frac{1}{4\sigma}\right)\left\|\nabla\left(u^{m+1}-u^m\right)\right\|^2\\
&\le\mathbb{E}\left(u^m,u^{m-1}\right).
\end{aligned}\tag{20}$$

Consequently, dropping some unnecessary terms, we can obtain

$$\mathbb{E}^{\alpha}\left(u^{m+1},u^{m}\right)\leq\mathbb{E}^{\alpha}\left(u^{m},u^{m-1}\right). \tag{21}$$

This completes the proof. □

Remark. The function

$$\begin{aligned}\mathbb{E}^{\alpha}\left(u^{m+1},u^{m}\right)&=E^{\alpha}\left(u^{m+1}\right)+\frac{1}{4\tau}\left\|u^{m+1}-u^{m}\right\|_{-1}^{2}\\&\quad+\frac{1}{2}\left\|u^{m+1}-u^{m}\right\|_{0}^{2}\end{aligned} \tag{22}$$

consists of three parts. The formula $E^{\alpha}(u^{m+1})$ comes from a typical free energy functional $E^{\alpha}(u)$. The formula $(1/4\tau)\|u^{m+1}-u^{m}\|_{-1}^{2}$ and $(1/2)\|u^{m+1}-u^{m}\|_{0}^{2}$ comes from the time difference term J_1 and the concave diffusive term J_4, respectively.

For the initialization scheme (7), we have the following stability result.

Theorem 2 (see [11]). *The initialization scheme (7) has the energy-decay property*

$$E^{\alpha}\left(u^{1}\right)\leq E^{\alpha}\left(u^{0}\right). \tag{23}$$

Moreover, we have the following mass conservation law.

Theorem 3. *For (1), the semidiscrete scheme (6) satisfies the mass conservation law:*

$$\mathbb{M}\left(u^{m+1}\right)=\mathbb{M}\left(u^{m}\right),\quad m=0,1,2,\ldots,M-1 \tag{24}$$

Proof. For m=0, it is easy to have $\mathbb{M}(u^1)=\mathbb{M}(u^0)$ based on Theorem 3.2. in [11].

For $m>0$, rewrite the scheme (6) as

$$\begin{aligned}&\frac{3u^{m+1}-4u^{m}+u^{m-1}}{2\tau}=\Delta\omega,\\&\omega\\&\quad=\left(\epsilon^{2}\left(-\Delta\right)^{\alpha/2}u^{m+1}+\left(u^{m+1}\right)^{3}-2u^{m}+u^{m-1}\right)\\&\qquad-A\tau\Delta\left(u^{m+1}-u^{m}\right).\end{aligned} \tag{25}$$

Then we have

$$\begin{aligned}\left(\frac{3u^{m+1}-4u^{m}+u^{m-1}}{2\tau},\mathbf{1}\right)&=\left(\Delta\omega,\mathbf{1}\right)=-\left(\nabla\omega,\nabla\mathbf{1}\right)\\&=0.\end{aligned} \tag{26}$$

Hence

$$3\left(u^{m+1}-u^{m},\mathbf{1}\right)=\left(u^{m}-u^{m-1},\mathbf{1}\right). \tag{27}$$

Then combined with the result $(u^0,1)=(u^1,1)$ (please see Theorem 3.2. in [11]), it is easy to verify that

$$\mathbb{M}\left(u^{m+1}\right)=\mathbb{M}\left(u^{m}\right). \tag{28}$$

This completes the proof. □

2.2. Spatial Discretization Using Spectral Methods. In this subsection, we will give the fully discrete scheme for model (1). We know that the fractional Laplacian $(-\Delta)^{\alpha/2}$ can be defined in various ways. A review of these existing definitions can be seen in [14]. One important and effective definition for $(-\Delta)^{\alpha/2}$ is defined using Fourier transform; see [15–17].

Without loss of generality, we set $\Omega=[a,b]^{d}$ and multi-index

$$\begin{aligned}\mu&=\left\{\left(p_1,p_2,\ldots,p_d\right)\mid p_i\in Z\right\}\\\mu^{+}&=\left\{p=\left(p_1,p_2,\ldots,p_d\right)\mid p_i\in N\right\}.\end{aligned} \tag{29}$$

Then, for $p\in\mu$, suppose the d-dimensional Laplacian $(-\Delta)$ has a complete set of orthonormal eigenfunctions φ_p corresponding to eigenvalues λ_p on the bounded region $[a,b]^{d}$, i.e., $(-\Delta)\varphi_p=\lambda_p\varphi_p$. Let

$$\begin{aligned}\mathcal{U}_{\alpha}=\Bigg\{&u=\sum_{l=1}^{d}\sum_{p_l=-\infty}^{\infty}\widehat{u}_p\varphi_p,\ \widehat{u}_p\\&=\left\langle u,\varphi_p\right\rangle,\ \sum_{l=1}^{d}\sum_{p_l=-\infty}^{\infty}\left|\widehat{u}_p\right|\left|\lambda_p\right|^{\alpha/2}<\infty,\Bigg\}.\end{aligned} \tag{30}$$

Then for any $u\in\mathcal{U}_{\alpha}$, it is easy to have

$$\left(-\Delta\right)^{\alpha/2}u=\sum_{l=1}^{d}\sum_{p_l=-\infty}^{\infty}\lambda_p^{\alpha/2}\widehat{u}_p\varphi_p, \tag{31}$$

where λ_p and φ_p will depend on the specified boundary conditions.

For periodic boundary condition,

$$\begin{aligned}\lambda_p&=\sum_{l=1}^{d}\left(\frac{2p_l\pi}{b-a}\right)^{2},\\\varphi_p&=\left(\frac{1}{b-a}\right)^{d/2}\prod_{l=1}^{d}\exp\left(i\frac{2p_l\pi\left(x-a\right)}{b-a}\right),\\&\qquad p\in\mu.\end{aligned} \tag{32}$$

Here, the imaginary unit is denoted by i.

For homogeneous Neumann boundary condition,

$$\begin{aligned}\lambda_p&=\sum_{l=1}^{n}\left(\frac{p_l\pi}{b-a}\right)^{2},\\\varphi_p&=\left(\frac{2}{b-a}\right)^{d/2}\prod_{l=1}^{d}\cos\left(\frac{p_l\pi\left(x-a\right)}{b-a}\right),\\&\qquad p\in\mu^{+}.\end{aligned} \tag{33}$$

In this work, we use (31) to handle the fractional Laplacian $(-\Delta)^{\alpha/2}$.

After discretizing governing equation in time as described in the above subsection, now we will further give the fully discrete scheme based on Fourier spectral method.

Table 1: The discrete L^2-norm errors and corresponding temporal convergence rates with $\alpha = 1.8$, $\epsilon^2 = 0.1$, $h = \pi/50$ and different numbers of fixed-point iterations L for Section 3.1.

L	τ	$\frac{1}{20}$	$\frac{1}{40}$	$\frac{1}{80}$	$\frac{1}{160}$	$\frac{1}{320}$
2	$\mathrm{Err}_\tau^{\tau/2}$	2.1916e-3	8.2837e-4	2.3878e-4	6.2590e-5	1.5914e-5
	Rate	-	1.40	1.79	1.93	1.98
4	$\mathrm{Err}_\tau^{\tau/2}$	2.1959e-3	8.2959e-4	2.3905e-4	6.2649e-5	1.5927e-5
	Rate	-	1.40	1.80	1.93	1.98
10	$\mathrm{Err}_\tau^{\tau/2}$	2.1959e-3	8.2959e-4	2.3905e-4	6.2649e-5	1.5927e-5
	Rate	-	1.40	1.80	1.93	1.80

Table 2: The same as in Table 1, but with $\alpha = 1.4$.

L	τ	$\frac{1}{20}$	$\frac{1}{40}$	$\frac{1}{80}$	$\frac{1}{160}$	$\frac{1}{320}$
2	$\mathrm{Err}_\tau^{\tau/2}$	1.1681e-2	5.6884e-3	1.8195e-3	4.9437e-4	1.2724e-4
	Rate	-	1.04	1.64	1.88	1.96
4	$\mathrm{Err}_\tau^{\tau/2}$	1.1687e-2	5.6882e-3	1.8190e-3	4.9414e-4	1.2717e-4
	Rate	-	1.04	1.64	1.88	1.96
10	$\mathrm{Err}_\tau^{\tau/2}$	1.1687e-2	5.6882e-3	1.8190e-3	4.9414e-4	1.2717e-4
	Rate	-	1.04	1.64	1.88	1.96

By applying the Fourier transform to both sides of (6), together with $f(u) = u^3 - u$, we have the following nonlinear scheme for the discrete p-th Fourier coefficients

$$\begin{aligned}\frac{\widehat{3u_p^{m+1} - 4u_p^m + u_p^{m-1}}}{2\tau} &= -\epsilon^2 \left(\lambda_p\right)^{1+\alpha/2} \widehat{u_p^{m+1}} \\ &\quad - \lambda_p \widehat{\left(u_p^{m+1}\right)^3} + 2\lambda_{pq} \widehat{u_p^m} \\ &\quad - \lambda_{pq} \widehat{u_p^{m-1}} \\ &\quad - A\tau \left(\lambda_p\right)^2 \left(\widehat{u_p^{m+1}} - \widehat{u_p^m}\right).\end{aligned} \tag{34}$$

For the nonlinear case, we need use an iterative method to solve the resulting algebraic system. Thus the above nonlinear term is treated using the following fixed point iteration: for $l = 1, 2, \ldots, L$ find $\widehat{u_p^{m+1,l}}$ such that

$$\begin{aligned}\widehat{u_p^{m+1,l}} &= \frac{1}{3 + 2\tau\epsilon^2 \left(\lambda_p\right)^{1+\alpha/2} + 2A\tau^2 \left(\lambda_p\right)^2} \Bigg[\Big(4 \\ &\quad + 4\tau\lambda_p + 2A\tau^2 \left(\lambda_p\right)^2 \Big) \widehat{u_p^m} - \left(1 + 2\tau\lambda_p\right) \widehat{u_p^{m-1}} \\ &\quad - 2\tau\lambda_p \widehat{\left(u_p^{m+1,l-1}\right)^3} \Bigg],\end{aligned} \tag{35}$$

with $\widehat{u_p^{m+1,0}} = \widehat{u_p^m}$.

It also preserves the mass conservation and energy dissipation properties in the full discrete sense. The proofs are similar. We thus omit them for simplicity.

3. Numerical Experiments

In this section, we investigate the performance of the obtained scheme (35). Four numerical experiments in 1D and 2D are carried out, some of the results are compared with the theoretical analysis from previous section, and all of them are consistent with the theoretical results.

3.1. Convergence Test. In order to verify the convergence rate of the proposed method, a 1D fractional CH problem (1) with homogeneous Neumann boundary condition is first considered. We take $\Omega = [-\pi, \pi]$, $T = 1$, $\epsilon^2 = 0.1$, and the initial condition $u_0(x) = 0.1\cos(x)$.

To test the accuracy of the numerical solutions, we choose a small grid size $h = 2\pi/100$ and calculate the L^2-norm error using $\mathrm{Err}_\tau^{\tau/2} = \|U^{\tau/2} - U^\tau\|_2$. We further estimate the rate of convergence using the formula as $\mathrm{Rate} = \log 2(\mathrm{Err}_\tau^{\tau/2}/\mathrm{Err}_{\tau/2}^{\tau/4})$.

The computational results corresponding to α=1.8, 1.4 are shown in Tables 1-2 for different time steps and numbers of fixed-point iterations L. One may see that the convergence rate in time is close to 2 for all cases, which was expected from the theoretical analysis in the previous section. Moreover, it is clear that the iteration number $L = 2$ in (35) is sufficient to get accurate results.

3.2. The Relationship among α, the Width of the Transition Layer, and the Equilibrium Solution. In this numerical experiment, we investigate the relationship among α, the width of the transition layer, and the equilibrium solution. We still use the same initial condition as in Section 3.1, and the simulation parameters are chosen as follows:

$$\epsilon^2 = 0.04,$$

$$T = 20,$$

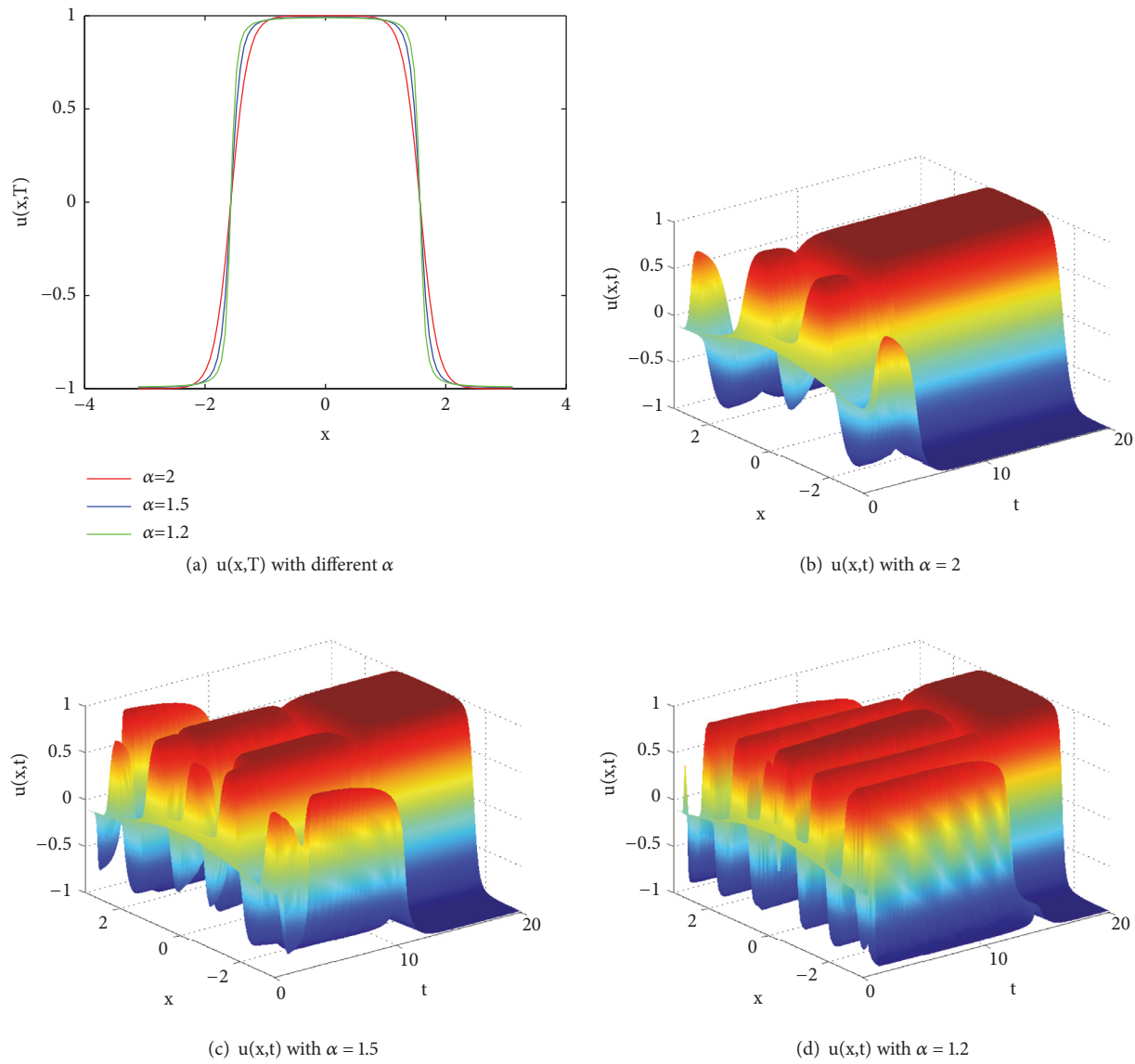

(a) u(x,T) with different α

(b) u(x,t) with $\alpha = 2$

(c) u(x,t) with $\alpha = 1.5$

(d) u(x,t) with $\alpha = 1.2$

FIGURE 1: Comparison of the interface widths and numerical solutions at T=20 with different α for Section 3.2.

$$h = \frac{\pi}{50},$$
$$\tau = \frac{1}{100},$$
$$L = 2. \tag{36}$$

Figure 1 shows the profiles of the phase-field at $t = 20$ and time evolution of solution for 1D fractional CH equation with α=2, 1.5, 1.2. We observe that small α can generate sharper interface than large α does; a similar phenomenon has also been found in [18] for the space fractional Allen-Cahn equation. Furthermore, due to the long-range dependence and the heavy-tailed influence of the fractional diffusion process, the lifetime of the unstable interface is largely prolonged as α decreases.

3.3. Effects on Phase Behavior of α and Boundary Conditions. In order to investigate effects on phase behavior of periodic and homogeneous Neumann boundary conditions, the third problem is considered on $(-1, 1)^2 \times (0, T]$ with both kinds of the boundary conditions and the following initial condition:

$$u_0(x, y) = \begin{cases} 1, & \text{if } (x - 0.5)^2 + (y - 0.5)^2 < \frac{1}{64}, \\ 1, & \text{if } (x + 0.5)^2 + (y + 0.5)^2 < \frac{1}{64}, \\ 0, & \text{else.} \end{cases} \tag{37}$$

The simulation parameters are chosen as follows:

$$\epsilon^2 = 0.01,$$
$$T = 20,$$

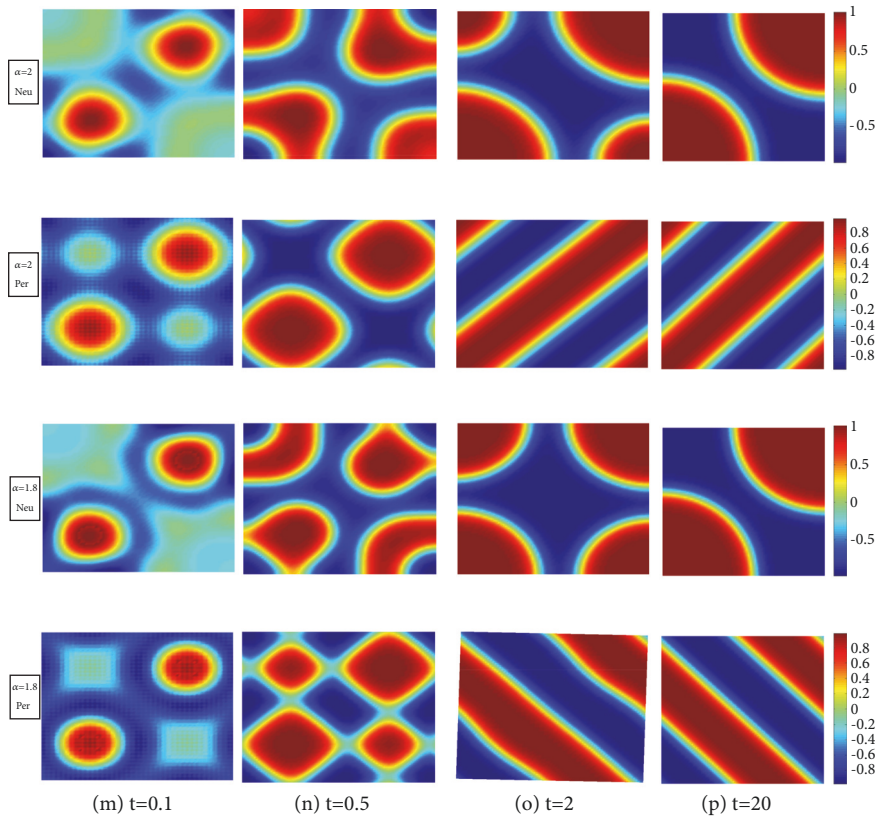

FIGURE 2: Section 3.3 for $\alpha = 2$ and $\alpha = 1.8$ with both boundary conditions: the first two rows for $\alpha = 2$ with periodic and Neumann boundary conditions, respectively; the next two rows for $\alpha = 1.8$ with periodic and Neumann boundary conditions, respectively.

$$h = \frac{1}{40},$$
$$\tau = \frac{1}{100},$$
$$L = 2. \tag{38}$$

For the 2D fractional CH equation, we study the coalescence dynamics of two separated bubbles by varying the fractional order α and boundary conditions. The snapshots of the solutions for both kinds of the boundary conditions and various values of α are shown in Figure 2. We observe that the solutions for different boundary conditions have significant differences and converge to different steady states. As α decreases, the interface thickness becomes thinner and the lifetime of the unstable interface is largely prolonged. For example, for $\alpha = 2$, the solution with periodic boundary condition has arrived the steady state at $t = 2$, whereas the solutions for $\alpha = 1.8$ are still unstable, which further support the results of Section 3.2 .

We also study three important physical quantities of the space fractional CH equation (1): the energy E^{α}, the mass M, and the surface roughness SR using the formula as

$$SR(t) = \sqrt{\frac{1}{|\Omega|}\int_{\Omega} \left|u(x,y,t) - \overline{u}(t)\right|^2 d\Omega},$$
$$\text{where } \overline{u}(t) = \frac{1}{|\Omega|}\int_{\Omega} u(x,y,t)\, d\Omega. \tag{39}$$

The corresponding quantities for both kinds of the boundary conditions and various values of α are shown in Figure 3, which represents the nonincreasing energy and conservation of mass of numerical solutions. Moreover, combined with the snapshots in Figure 2, we observe that for the space fractional CH equation (1) with periodic boundary condition, the time to reach steady state is much shorter than problem (1) with periodic boundary condition. For example, the energy curves in Figure 3 indicate that the solutions with periodic boundary condition arrive the steady state at around $t = 1.8$ for $\alpha = 2$ (see Figure 3(d)) and $t = 2.5$ for $\alpha = 1.8$ (see Figure 3(j)), respectively whereas the solution with Neumann boundary condition is stable at around $t = 6$ for $\alpha = 2$ (see Figure 3(a)) and $t = 17$ for $\alpha = 1.8$ (see Figure 3(g)). This phenomenon is in good agreement with that reported in [11]. Meanwhile, the above results show again that the lifetime of the unstable interface is largely prolonged as the fractional order α decreases.

3.4. Comparison of Different Methods. Moreover, for comparison purpose we review an alternative numerical method [11],

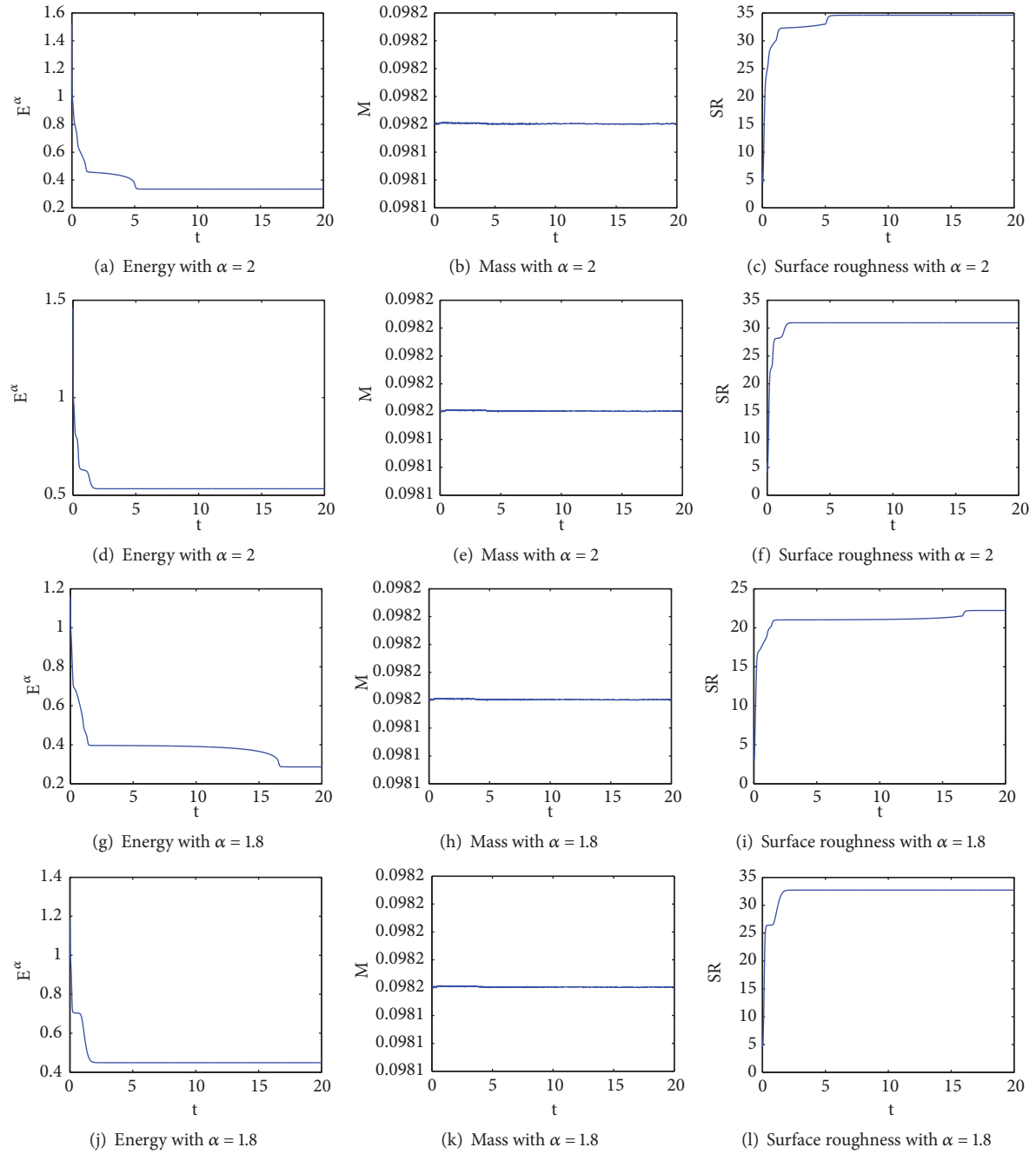

FIGURE 3: Section 3.3 for the curves of energy, mass, and surface roughness computed with $h = 1/40$ and $\tau = 1/100$: the first two rows, respectively, for Neumann and periodic boundary conditions with $\alpha = 2$; the next two rows, respectively, for Neumann and periodic boundary conditions with $\alpha = 1.8$.

which is an unconditionally energy stable Crank-Nicolson (CN) scheme for space fractional CH equation (1):

$$\frac{\widehat{u_{pq}^{m+1}} - \widehat{u_{pq}^{m}}}{\tau} = \frac{1}{2}\left(-\lambda_{pq}\widehat{\left(u_{pq}^{m}\right)^{3}} + \lambda_{pq}\widehat{u_{pq}^{m}} - \epsilon\lambda_{pq}^{1+\alpha/2}\widehat{u_{pq}^{m}} - \lambda_{pq}\widehat{\left(u_{pq}^{m+1}\right)^{3}} + \lambda_{pq}\widehat{u_{pq}^{m+1}} - \epsilon^{2}\lambda_{pq}^{1+\alpha/2}\widehat{u_{pq}^{m+1}}\right) + \frac{1}{4} \cdot \lambda_{pq}\widehat{\left(u^{m+1} - u^{m}\right)^{2}\left(u^{m+1} + u^{m}\right)}. \tag{40}$$

For this scheme, the spatial and temporal discretization errors are also of spectral and second-order accuracy, respectively.

Since the time to reach steady state for model (1) with periodic boundary condition is much shorter than the Neumann case (as shown in Section 3.3), we only consider the periodic boundary condition for convenient comparison. The

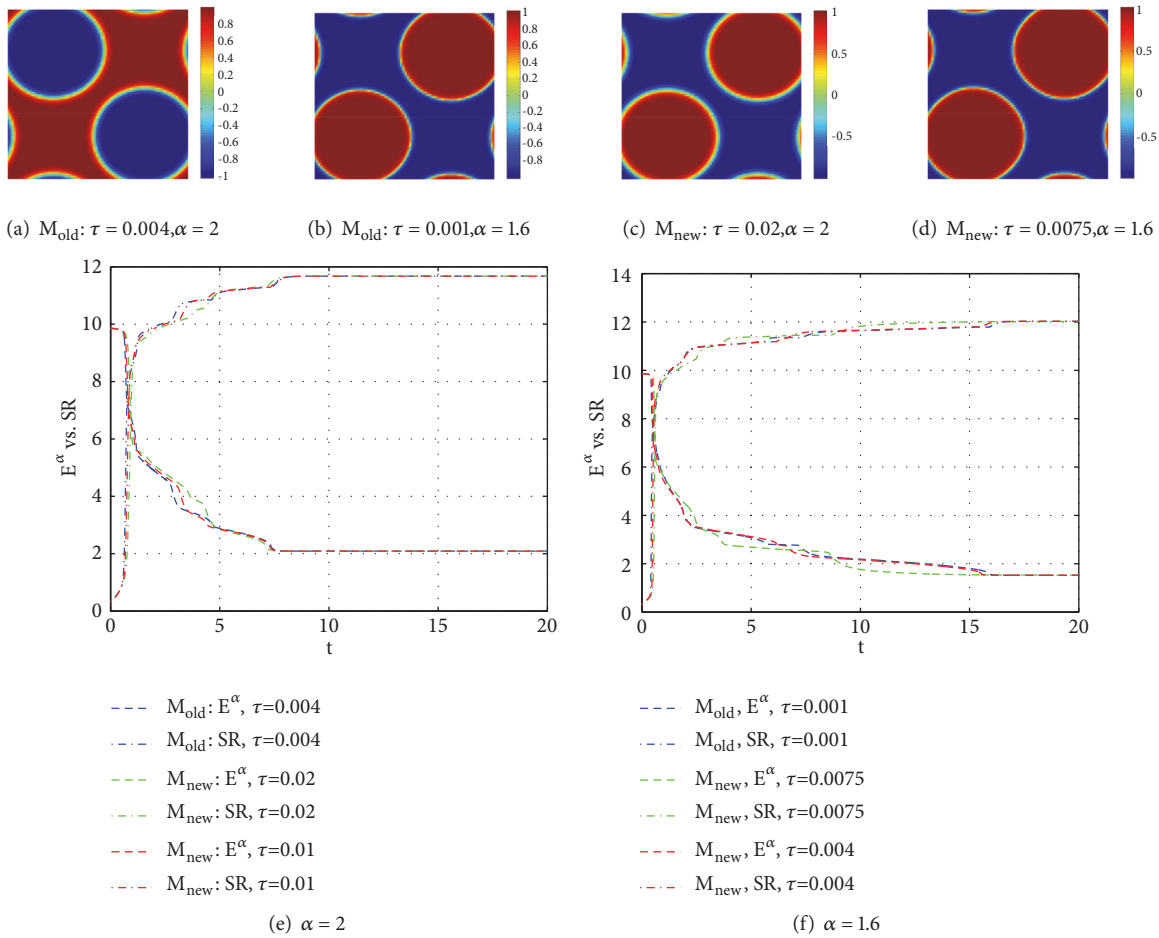

FIGURE 4: Comparison of the numerical solutions at T=20 and E^α, SR with different α and τ for Section 3.4.

TABLE 3: A comparison of the CPU time (in seconds) used by our scheme (35) (denoted by M_{new}) and the method in [11] (denoted by M_{old}).

	α=2					α=1.6				
	M_{old}		M_{new}			M_{old}		M_{new}		
τ	≥ 0.005	0.004	> 0.02	0.02	0.01	≥ 0.0013	0.001	> 0.0075	0.0075	0.004
Convergence	No	Yes	No	Yes	Yes	No	Yes	No	Yes	Yes
CPU	-	89.8	-	10.5	20.0	-	332.4	-	28.6	52.0

fourth problem from [11, 19] with $\epsilon^2 = 0.01$ is considered on $(0, 2\pi)^2 \times (0, 20]$ with the following initial condition

$$u_0(x, y) = 0.05 \sin(x) \sin(y) + 0.001. \quad (41)$$

In this test, we fix the spatial step $h = 2\pi/80$. In order to compare the performance of our method (denoted by M_{new}) with the method (40) (denoted by M_{old}), the numerical results and the computational times (in seconds) for different α are presented in Table 3. It is observed that the scheme M_{old} is not convergence when $\tau \geq 0.0013$ for $\alpha = 2$ and $\tau \geq 0.005$ for $\alpha = 1.6$, whereas our scheme M_{new} can work well even with τ=0.02 for $\alpha = 2$ and τ=0.0075 for $\alpha = 1.6$. This further suggests that the obtained scheme in this paper can lead to a substantial reduction of the CPU time, while keeping high accuracy of the computed solution.

The numerical solutions at $t = 20$ are presented in Figures 4(a)–4(d), it is clear that the interface thickness becomes thinner as the fractional power is decreased. Besides that fact that both methods (35) and (40) reach the same equilibrium solution, only the scheme (40) arrives to an inverse equilibrium solution for $\alpha = 2$ (of course, the surface area of all numerical solutions reached the minimum value.). As a conclusion we claim that from the computational point of view, the scheme (35) is better than (40) because we can take bigger time steps (reducing the computational cost) and still obtain a good behavior of the scheme.

Figures 4(e) and 4(f) show the evolution of the free energy E^α and surface roughness SR in time for both schemes. The energies and roughnesses do not evolve in the same way but all of them reach the same equilibrium states. Furthermore,

with the decrease of the time steps, the dynamic of E^{α} and SR for scheme (35) is almost the same for (40).

Remark. From Table 1 we find that the critical time step for $\alpha = 1.6$ is much smaller than that of $\alpha = 2$. We would like to comment with the fact that since the thickness of the interface is inversely proportional to α (see Figures 4(a)–4(d)), the case for small α requires a finer time step. In addition, since phase-field models tend to sharp-interface models as the thickness of the interfaces tends to zero; this case is more interesting from the physical point of view.

4. Conclusions

In this work, we have presented a second order BDF-type scheme in time to solve fractional-in-space CH model. The energy stability and mass conservation of the semi-discrete scheme have been proved. Moreover, the space has been discretized by Fourier spectral method. Several numerical examples have verified our theoretical results. Via numerical comparison, we have shown that, by introducing a second-order Douglas-Dupont-type regularization based on the implicit backward difference scheme, larger time step can also guarantee stability and accuracy. We observe from the numerical results the lifetime of the unstable interface is largely prolonged as the fractional order α decreases and small α can generate sharper interface.

Data Availability

The data of numerical experiment in the manuscript used to support the findings of this study are included within the article.

Conflicts of Interest

The authors declare that they have no conflicts of interest.

Acknowledgments

This work of Zhifeng Weng is in part supported by the Natural Science Foundation of China (no. 11701197), and the research of Langyang Huang is in part supported by the Natural Science Foundation of China (no. 11701196) and Progmotion Program for Young and Middle-Aged Teacher in Science and Technology Research of Huaqiao University (ZQN-YX502).

References

[1] J. W. Cahn and J. E. Hilliard, "Free energy of a nonuniform system. I. Interfacial free energy," *The Journal of Chemical Physics*, vol. 28, no. 2, pp. 258–267, 1958.

[2] J. W. Cahn, "On spinodal decomposition in cubic crystals," *Acta Metallurgica et Materialia*, vol. 10, no. 3, pp. 179–183, 1962.

[3] Q. Du and R. A. Nicolaides, "Numerical Analysis of a Continuum Model of Phase Transition," *SIAM Journal on Numerical Analysis*, vol. 28, no. 5, pp. 1310–1322, 1991.

[4] Q. Du, C. Liu, and X. Wang, "Simulating the deformation of vesicle membranes under elastic bending energy in three dimensions," *Journal of Computational Physics*, vol. 212, no. 2, pp. 757–777, 2006.

[5] P. Yue, J. J. Feng, C. Liu, and J. Shen, "A diffuse-interface method for simulating two-phase fows of complex fuids," *J. Fluid Mech*, vol. 515, pp. 293–317, 2004.

[6] J. Shen and X. Yang, "An efficient moving mesh spectral method for the phase-field model of two-phase flows," *Journal of Computational Physics*, vol. 228, no. 8, pp. 2978–2992, 2009.

[7] X. Feng and A. Prohl, "Error analysis of a mixed finite element method for the Cahn-Hilliard equation," *Numerische Mathematik*, vol. 99, no. 1, pp. 47–84, 2004.

[8] J. Bosch and M. Stoll, "A fractional inpainting model based on the vector-valued cahn–hilliard equation," *SIAM Journal on Imaging Sciences*, vol. 8, no. 4, pp. 2352–2382, 2015.

[9] M. Ainsworth and Z. Mao, "Analysis and approximation of a fractional cahn–hilliard equation," *SIAM Journal on Numerical Analysis*, vol. 55, no. 4, pp. 1689–1718, 2017.

[10] M. Ainsworth and Z. Mao, "Well-posedness of the Cahn–Hilliard equation with fractional free energy and its Fourier Galerkin approximation," *Chaos, Solitons & Fractals*, vol. 102, pp. 264–273, 2017.

[11] Z. Weng, S. Zhai, and X. Feng, "A Fourier spectral method for fractional-in-space Cahn–Hilliard equation," *Applied Mathematical Modelling*, vol. 42, pp. 462–477, 2017.

[12] H. Liu, A. Cheng, H. Wang, and J. Zhao, "Time-fractional Allen–Cahn and Cahn–Hilliard phase-field models and their numerical investigation," *Computers & Mathematics with Applications*, vol. 76, no. 8, pp. 1876–1892, 2018.

[13] Y. Yan, W. Chen, C. Wang, and S. M. Wise, "A second-order energy stable bdf numerical scheme for the cahn-hilliard equation," *Communications in Computational Physics*, vol. 23, pp. 572–602, 2018.

[14] W. Chen and G. Pang, "A new definition of fractional Laplacian with application to modeling three-dimensional nonlocal heat conduction," *Journal of Computational Physics*, vol. 309, pp. 350–367, 2016.

[15] S. Zhai, Z. Weng, and X. Feng, "Fast explicit operator splitting method and time-step adaptivity for fractional non-local Allen-Cahn model," *Applied Mathematical Modelling: Simulation and Computation for Engineering and Environmental Systems*, vol. 40, no. 2, pp. 1315–1324, 2016.

[16] A. Bueno-Orovio, D. Kay, and K. Burrage, "Fourier spectral methods for fractional-in-space reaction-diffusion equations," *BIT Numerical Mathematics*, vol. 54, no. 4, pp. 937–954, 2014.

[17] S. Zhai, Z. Weng, and X. Feng, "Investigations on several numerical methods for the non-local Allen–Cahn equation," *International Journal of Heat and Mass Transfer*, vol. 87, pp. 111–118, 2015.

[18] F. Song, C. Xu, and G. E. Karniadakis, "A fractional phase-field model for two-phase flows with tunable sharpness: Algorithms and simulations," *Computer Methods Applied Mechanics and Engineering*, vol. 305, pp. 376–404, 2016.

[19] X. Feng, T. Tang, and J. Yang, "Long time numerical simulations for phase-field problems using p-adaptive spectral deferred correction methods," *SIAM Journal on Scientific Computing*, vol. 37, no. 1, pp. 271–294, 2015.